

---

## Tunning Spin Hall conductivities in GeTe by Ferroelectric Polarizations

Wenxu Zhang<sup>1\*</sup>, Zhao Teng<sup>1</sup>, Huizhong Zeng<sup>1</sup>, Jakub Železný<sup>2</sup>, Hongbin Zhang<sup>3</sup>, and Wanli Zhang<sup>1</sup>

<sup>1</sup>State Key Laboratory of Electronic Thin Films and Integrated Devices, University of Electronic Science and Technology of China, Chengdu, 610054, P. R. China

<sup>2</sup>Institute of Physics, Czech Academy of Sciences, Cukrovarnická 10, 16000 Prague 6, Czech Republic

<sup>3</sup>Institute of Materials Science, Technische Universität Darmstadt, Darmstadt, 64287, Germany

**Keywords:** ferroelectric semiconductors, spin Hall effects, spin orbital coupling, Rashba effects

Controlling charge-spin current conversion by electric fields is crucial in spintronic devices, which can be realized in diatom ferroelectric semiconductor GeTe where it is established that ferroelectricity can change the spin texture. We demonstrated that the spin Hall conductivity (SHC) can be further tuned by ferroelectricity based on the density functional theory calculations. The spin texture variation driven by the electric fields was elucidated from the symmetry point of view, highlighting the interlocked spin and orbital degrees of freedom. We observed that the origin of SHC can be attributed to the Rashba effect and the intrinsic spin orbit coupling. The magnitude of one component of SHC  $\sigma_{xy}^z$  can reach as large as  $100 \hbar/e(\Omega\text{cm})^{-1}$  in the vicinity of the band edge, which is promising for engineering spintronic devices. Our work on tunable spin transport properties via the ferroelectric polarization brings noval assets into the field of spintronics.

### I. Introduction

Spintronics is a multidisciplinary subject where the coupling of the spin and orbital degrees of freedom for electrons plays a vital role. The most magnificent demonstration of such a coupling is the conversion of charge current into spin current, i.e., spin Hall effect (SHE). Such a phenomenon has be measured in many different material systems, such as heavy metals<sup>[1]</sup>, semiconductors<sup>[2]</sup>, and interfaces between oxides such as LAO/STO<sup>[3]</sup>. Manipulation of the charge-spin conversion is one of the keys to future implementation of spintronic devices<sup>[4-5]</sup>. The

---

controllable spin-orbit coupling leading to a gateable electric signal in LAO/STO has been observed by several groups, as reviewed by Han *et al.*<sup>[6]</sup>. The underlying mechanism is the change of the electron density and hence the occupation of different orbitals<sup>[7]</sup>.

Very recently, another material family was proposed to show electrically controllable spin-orbit coupling based on ferroelectricity, called ferroelectric Rashba semiconductors (FERSC). These materials include GeTe<sup>[8-9]</sup>, SnTe<sup>[10]</sup> and MX<sub>2</sub><sup>[11]</sup> etc. Among them, GeTe, a narrow gap semiconductor, has drawn intensive attention due to a spectrum of interesting properties such as thermoelectricity<sup>[12]</sup>, ferroelectricity<sup>[13-15]</sup>, and electrical phase change<sup>[16]</sup>, realized within such simple stoichiometry and the two-atom rhombohedral unit cell<sup>[17]</sup>. Both experiments and theoretical calculation show that the strength of Rashba coupling in GeTe can be tailored by the electric polarization. Meanwhile, the spin texture can also be fine-tuned by the electric polarization as revealed by theoretical calculations<sup>[9]</sup> based on the density functional theory (DFT) and spin resolved ARPES<sup>[18]</sup>: The clockwise winding directions in the reciprocal space of the spin vectors can be reversed to anticlockwise. There are several other ferroelectric compounds which show the reversible spin texture controlled by electric polarization, such as HfO<sub>2</sub><sup>[19]</sup>, BiTeI<sup>[20]</sup>, and GeTe/InP superlattice<sup>[21]</sup>. The controllable spin texture may lead to tunable spin life time, so that the proposed spin transistor<sup>[4]</sup> may be realized, as in the recently demonstrated ferromagnetic-free all-electric spin Hall transistor<sup>[5]</sup>. Although it is well established that the spin texture can be tuned by the polarization by the ARPES and DFT calculations, it is still not clear how the spin-charge current conversion is influenced. Such a tunable conversion is the crucial to utilize the effect in real devices. For instance, the spin-charge conversion in GeTe was observed by Rinaldi *et al.*<sup>[22]</sup> for the first time very recently, but the tuning of the conversion efficiency has not been reported yet.

---

In this work, we elaborate by *ab initio* calculations, as well as by general arguments based on the effect of electric polarization on the spin texture, that the electric fields can be applied to modulate the spin Hall conductivity (SHC), which is originated from both the Rashba effect caused by polarization and the bulk effect. It is observed that the bulk effect is only marginally influenced, while the magnitude of the Rashba effect near the band edge change significantly under ferroelectric distortions with even a sign change. Thus, it leads to tunable SHC, which opens the door for spintronics.

## II. Calculation Details

GeTe crystallizes into the noncentrosymmetric rhombohedral structure (space group R3m, No. 160) with rhombohedral lattice constant  $a = 4.373 \text{ \AA}$  and the angle  $\alpha$  between the axis  $57.76^\circ$ . Ferroelectric polarization is realized by the relative displacement of Ge and Te along the [111]-direction which is chosen as the  $z$ -axis in our calculations. The lattice parameters are fully relaxed when the polarization is changed. The electronic structure was calculated by the psuedo-potential plane wave method (PWscf)<sup>[34]</sup> within the generalized gradient approximation (GGA) parameterized by Perdew *et al.*<sup>[35]</sup>. The energy cut-off was set to 30 Ry and the Brillouzin zone integration was performed on a uniform  $k$ -grid with  $20 \times 20 \times 20$   $k$ -points. The electronic structure analyse was carried out by the graphic interface VNL<sup>[36]</sup>. The Hilbert space with the plane wave basis was projected onto the maximally localized Wannier orbital spaces spanned the valence  $s$ - and  $p$ -orbitals. Calculations of the spin Hall conductivity was performed by the code developed by one of the authors<sup>[37]</sup>, which evaluates the Kubo formula within the linear response theory. The intrinsic SHC can be obtained with the help of Berry curvature<sup>[33]</sup>, which has the following form

$$\sigma_{\alpha\beta}^{\gamma} = \frac{e}{\hbar} \sum_n \int_{BZ} \frac{d^3 \vec{k}}{(2\pi)^3} f_n(\vec{k}) \Omega_{n,\alpha\beta}^{\gamma}(\vec{k}), \quad (1)$$

---

where  $\Omega_{n,\alpha\beta}^\gamma(\vec{k})$  is referred to as the spin Berry curvature defined as

$$\Omega_{n,\alpha\beta}^\gamma(\vec{k}) = 2i\hbar^2 \sum_{m \neq n} \frac{\langle u_n(\vec{k}) | \hat{J}_\alpha^\gamma | u_m(\vec{k}) \rangle \langle u_n(\vec{k}) | \hat{v}_\beta | u_m(\vec{k}) \rangle}{(\epsilon_n(\vec{k}) - \epsilon_m(\vec{k}))^2}, \quad (2)$$

with  $\alpha, \beta, \gamma = x, y, z$ , and  $m, n$  being the band indices. The spin current operator is  $\hat{J}_\alpha^\gamma =$

$\frac{1}{2} \{ \hat{v}_\alpha, \hat{\sigma}_\gamma \}$ , where  $\hat{\sigma}_\gamma$  is the spin operator component  $\gamma$ . The Fermi Dirac distribution

function  $f_n(\vec{k})$  is the mean occupation number of state  $n(\vec{k})$  at a finite temperature  $T$ . In

this work, we set  $T = 0$  K. The third-order tensor  $\sigma_{\alpha\beta}^\gamma$  represents the spin current  $J_{S_\alpha}^\gamma$

generated by an electric field  $\vec{D}$  via  $J_{S_\alpha}^\gamma = \sigma_{\alpha\beta}^\gamma D_\beta$ . The spin current is polarized in the  $\gamma$

direction and flows in the  $\alpha$ -direction, for an electric field applied in the  $\beta$ -direction.

The integral over the  $k$ -space during the calculation of the SHC was sampled in the first BZ with grids of  $200 \times 200 \times 200$  to ensure the convergence. The unit of SHC is  $\hbar/e(\Omega\text{cm})^{-1}$

### III Results and discussions

#### A. Electronic Structure and Ferroelectricity

The Kohn-Sham band structure calculated using the experimental lattice constants is shown in Fig. 1, where also a comparison of the results with and without SOC is made. Without SOC, the ferroelectric distortion leads to the direct band gap of about 0.66 eV near the  $L$ -point as depicted by the dashed blue curves. The value is only 0.05 eV higher than the experimental value reported by Park *et al.*<sup>[23]</sup>. We note that even in the absence of SOC, there are humps around the  $L$ -point due to the finite electric polarization. SOC leads to splitting ( $\Delta_{\text{SOC}}$ ) of the bands about 0.7 eV along the  $\Gamma$ - $L$  line, which indicates that the SOC field is more or less collinear in this direction. However, the Rashba like splitting are only around

the  $L$ -point, and mostly obvious at the VBM at  $L$  as shown by the solid red lines. This direction is in the direction of polarization in our coordinate system. The contributions of the SOC are mainly observed in the valence bands due to the fact that they are mostly originated from the Te  $5p$ -orbitals, while the conduction bands are from the Ge  $2p$ -orbitals. This is in contrast to a simple interpretation of resonant bonds, because the  $5p$ -states of Te is much higher in energy than the  $2p$ -states of Ge. The so-called “cross gap hybridization” was used to depict this phenomenon in the highly ionic compound<sup>[24-25]</sup>. This anomaly is related to the enhanced Born effective charge which in turn improves the bonding with distortion.

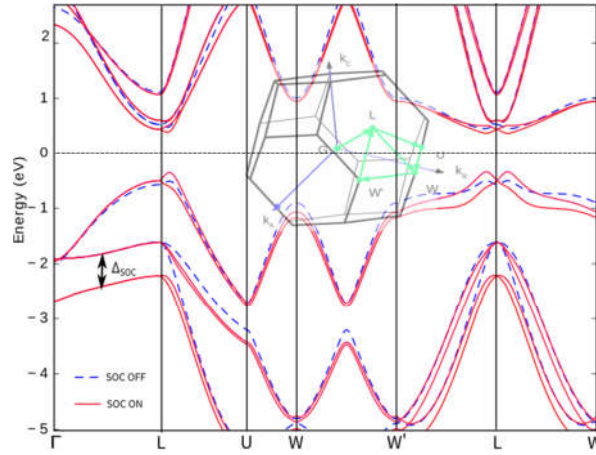


FIG. 1. (color online) Comparison of the Kohn-Sham band structure of GeTe without (dashed blue curves) and with SOC (solid red curves). The vertical double arrow indicates the SOC splitting of the states  $\Delta_{SOC}$  along the  $\Lambda$ -line. The inset shows the path and the special  $k$ -points in the Brillouin Zone used in the calculations.

The spin-dependent fat bands are shown in Fig. 2. The band dispersions for reversed polarizations, namely  $+P$  and  $-P$ , are the same. This is understandable because the ferroelectric displacement and spin- $z$  directions are the same. If the SOC is neglected, the spin polarization should be independent of the crystal coordinates. In this case, the spins

---

are unaltered upon electric polarization reversal. At the  $L$ -point, the spin vectors in the  $X$  and  $Y$  directions have different contributions when the  $k$ -path is along  $L - U$  and  $L - A$  directions as shown in Fig.2(a) and (c). These contributions are reversed when the polarization is reversed from  $+P$  to  $-P$ . As a result, the winding directions of the spin vectors are reversed in the  $k$ -space as reported in previous works<sup>[9]</sup> due to the SOC. We noticed that there is no  $x$  nor  $y$ -components contributions along  $\Gamma - L$  coincided with the collinear SOC field in this direction as shown previously. This leads to an almost rigid shift of the bands along this direction as discussed. At the same time, we plotted the  $z$ -component of the spin in Fig. 2 (b) and (d). It can be seen that the different polarization also changes the projection weight. The changing of the spin winding direction can be understood as following: In the real space, the polarization reversal is equivalent to change the  $z$ -component of the coordinate system. In this case, the  $x$ - $y$  axis changes from the right-handed to the left-handed as the view points are changed from the  $z$  to  $-z$ -axis. This effect is universal in ferroelectric materials as it is related to the changing of the coordinate system once the polarization reversal is realized only by the relative shift of the atomic positions. This effect can also be clearly seen from the electron isosurface of the different spin components as in Fig. 3. In the figure, we show the negative polarization in a cell which is rotated up-side-down, so that the atomic positions are the same as shown by (a) and (b). As observed from the figure, in this case, the spin densities of  $x$ ,  $y$  and  $z$ -components are the same, so that the spin directions are the same. However, the  $z$ -axis of the coordinates is reversed, which gives the polarization direction. This is the way by which the spin directions are interlocked with ferroelectric polarizations.

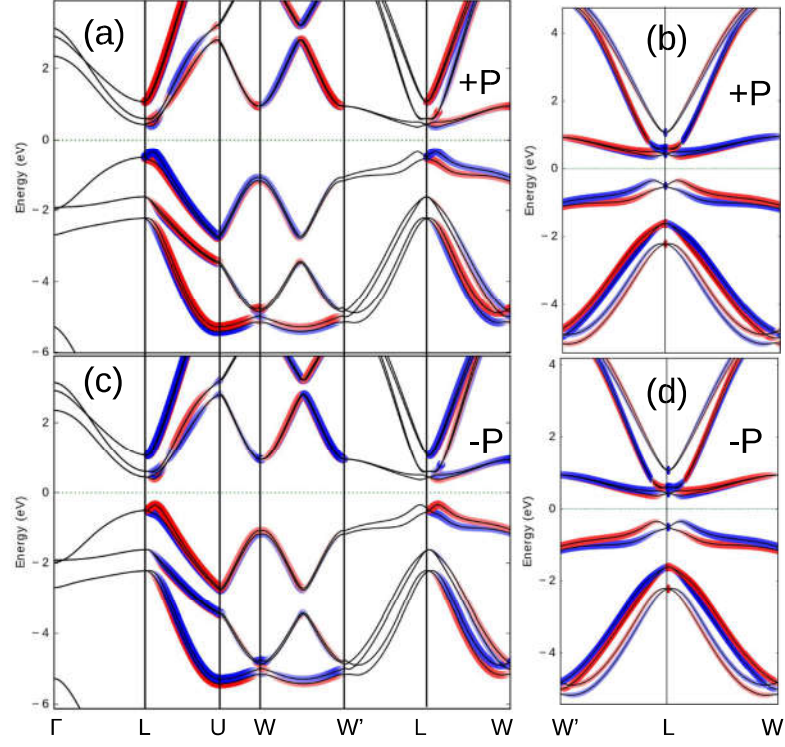


FIG. 2. The spin component weighted band structure of GeTe with polarization of  $+P$  weighted by  $x$ - (a) and  $z$ -components (b) together with  $-P$  by  $y$ - (c) and  $z$ -components (d).

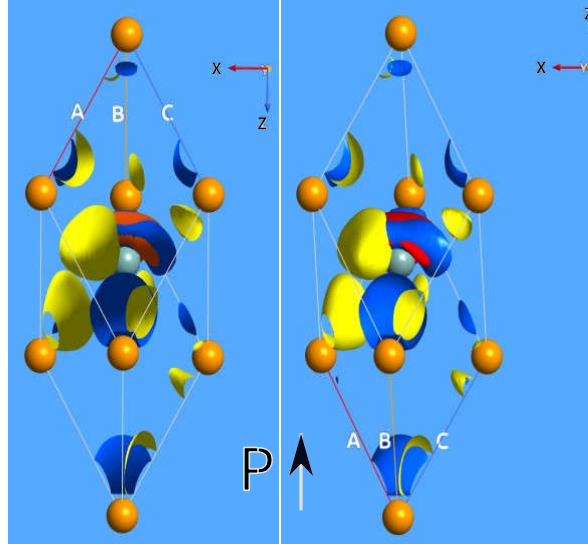


FIG. 3. (Color online) The electron isosurface of different spins with ferroelectric polarization  $+P$  (a) and  $-P$  (b). Noticed that in the two subfigures, the polarization are plotted in the same directions while the  $z$ -axis of coordinate system is turned upside down

---

## B. Spontaneous Polarization and Rashba Coupling

The ferroelectricity in GeTe was well explored and understood more than fifty years ago<sup>[26-27]</sup>. The soft optical phonon is the cause of the displacive movement of the diatomic compound. In GeTe, ferroelectric displacement of Te along [111] shows double well energy minimums at  $\tau = 0.03 a_0$  away from the middle point the diagonal, where  $a_0$  is the lattice parameter. The potential barrier height is about 54 meV, which is twice as large as that of BaTiO<sub>3</sub> and half the value of PbTiO<sub>3</sub><sup>[28]</sup>. This is reflected by the fact that the Curie temperature of GeTe is about 670 K, lying between those of BaTiO<sub>3</sub> and PbTiO<sub>3</sub>. The spontaneous ferroelectric polarization of 67  $\mu\text{C}/\text{cm}^2$  is obtained by the Berry phase theory of polarization<sup>[29]</sup>. The Born effective charge ( $Z^*$ ) is estimated by the finite difference method from the expression

$$\delta P = \frac{e}{\Omega} Z^* \cdot \delta u. \quad (3)$$

where  $\delta u$  is the first-order change of the positions of Te and  $\Omega$  is the volume of the unit cell. We estimate the  $Z^*$  is about 9.58  $e$  from the data when  $u$  is below 0.1 Å. This is a large value at the same scale of other ferroelectric compounds indicating the strong interactions of the orbitals between Te and Ge along the [111]-direction.

In ferroelectric materials, the electric field will induce displacement of the ions and the electronic structure will change accordingly as shown in Fig. 4. The nonlinearity and asymmetry is apparent when the electric field gets larger in the two different directions. The Zener breakdown field  $E_{Zb}$  is estimated to be  $E_{Zb} = E_g/L \sim 0.01 \text{ a.u.} = 51 \text{ MV/cm}$ , where  $E_g$  is the band gap and  $L$  is the length of the unit cell in the direction of the electric field. In our calculations, the maximum field strength is about one order smaller than the breakdown field in order to avoid such an instability. As expected when the field is along



the direction of polarization, the Rashba splitting  $E_R$  follows a linear behavior of the electric field ( $\vec{D}$ ) as understood by the Bychkov-Rashba Hamiltonian

$$H_R = \alpha_R(|\vec{D}|)\vec{\sigma} \cdot (\vec{k}_{\parallel} \times \vec{e}_z) \quad (4)$$

Where  $\vec{k}_{\parallel} = (k_x, k_y, 0)$  and  $\vec{e}_z = (0, 0, 1)$ . The nature of the phenomenon allows us to use the free two-dimensional electron gases(2DEG) model to get the related parameters. The spin degeneracy of the 2DEG is lifted and the energy dispersion has the form

$$E_{RSO} = \frac{\hbar^2}{2m^*} \left( |\vec{k}_{\parallel}| \pm k_R \right)^2 - E_R. \quad (5)$$

The Rashba parameter  $\alpha_R$ , which is related to  $E_R$  and  $k_R$  by  $\alpha_R = 2E_R/k_R$ , is proportional to the electric field  $\vec{D}$ . From our calculations, the  $E_R$ ,  $k_R$  and  $\alpha_R$  are estimated to be 0.24 eV, 0.10 Å<sup>-1</sup> and 4.8 eV Å, respectively, when the field is not applied. The Rashba parameter  $\alpha_R$  is comparable with the experiments<sup>[30]</sup> and also previous theoretical calculations<sup>[9]</sup>.

### C. SHC and its dependence on the ferroelectric polarization

Since the intrinsic SHC is determined fully by the band structure, it is compatible with the point group symmetry of the Hamiltonian. We therefore use the symmetry analysis code<sup>[31]</sup> to figure out the nonzero matrix elements in order to simplify the computation of the third-order tensors. Due to the symmetry constraints, there are only four nonzero elements  $\delta_i$  ( $i = 0, 1, 2$ , and 3). The full SHC tensors are listed as following:

$$\sigma^x : \begin{pmatrix} \delta_0 & 0 & 0 \\ 0 & -\delta_0 & -\delta_1 \\ 0 & -\delta_2 & 0 \end{pmatrix}, \sigma^y : \begin{pmatrix} 0 & -\delta_0 & \delta_1 \\ -\delta_0 & 0 & 0 \\ \delta_2 & 0 & 0 \end{pmatrix}, \text{ and } \sigma^z : \begin{pmatrix} 0 & -\delta_3 & 0 \\ \delta_3 & 0 & 0 \\ 0 & 0 & 0 \end{pmatrix} \quad (6)$$

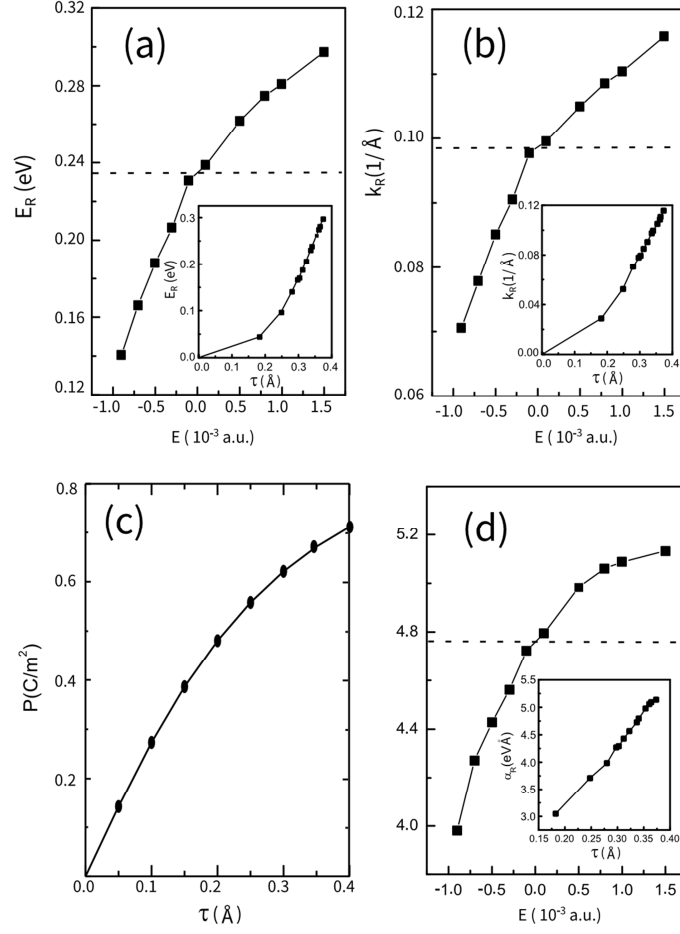


FIG. 4. The variations of the parameters ( $E_R$ (a),  $k_R$ (b) and  $\alpha_R$ (d)) defined in the Rashba model with the electric field and the electric polarizations as the function of the ferroelectric displacements  $\tau$  (c).

The non-zero elements are calculated at the stationary state with ferroelectric polarization are shown in Fig. 5. All the tensor components are of the same order of magnitude about  $100 \hbar/e(\Omega\text{cm})^{-1}$  around the conduction band minimum (CBM) and valence band maximum (VBM). Interestingly, the charge current  $I$  and spin polarization  $J_s$  are not necessary perpendicular to each other. There are sizable contributions from the  $\delta_0$ , namely  $\sigma_{xx(yy)}^z$  and  $\sigma_{xy(yx)}^z$ , which means that we can get longitudinal spin Hall signal when the spin polarization is in plane and perpendicular to the electric polarization. This value is

peaked when the Fermi energy is about 1.1 eV above the CBM. This feature gives us more freedom to design spintronic devices. The  $\sigma_{xy}^z$  is negative around the CBM and VBM. Recent experiments by Rinaldi *et al.*<sup>[22]</sup> reveals that the charge current produced by the spin current in GeTe is opposite to that found in Pt. As we know, the SHC calculated in Pt<sup>[32]</sup> at the Fermi level is  $2200 \hbar/e(\Omega\text{cm})^{-1}$ , which is in good agreement with the experiments<sup>[33]</sup>. Thus the sign of SHC is in agreement with the experiment, however, its magnitude has not been measured yet in GeTe.

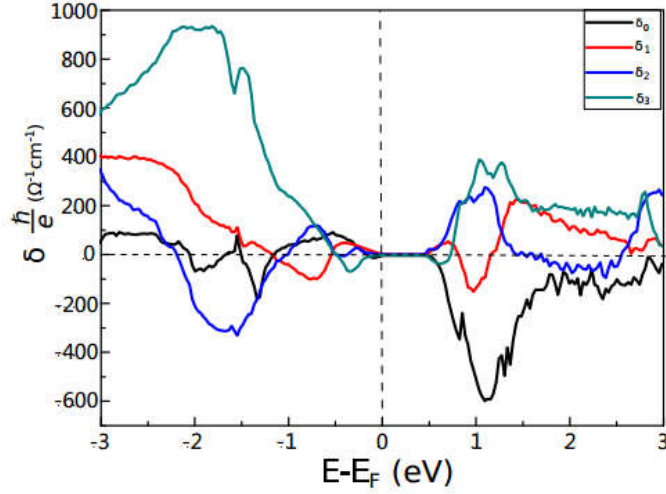


FIG. 5. (Color online) Components of the spin Hall conductivity tensor as a function of the Fermi level.

The SHC as a function of the Fermi level is shown in Fig. 5. The SHC has the same signs for the electron and hole doping as seen in the figure. The maxima at the VBM and CBM are about  $-100 \hbar/e(\Omega\text{cm})^{-1}$  which are mainly due to the Rashba effect, in the sense that it is sensitively dependent on the electric polarization as can be seen in the following discussions. We see there is much larger SHC amounting  $900 \hbar/e(\Omega\text{cm})^{-1}$  around 2 eV below the VBM. When comparing with the band structure in Fig. 1, we notice that there is a

---

large SOC splitting ( $\Delta_{soc}$ ) about 0.7 eV for the bands within this energy range. We suspect that the enhanced SHC is caused by the large splitting of the bands induced by SOC.

The dependence of SHC with respect to the electric polarization can be seen in Fig.6, where the SHC is evaluated at several ferroelectric displacements ( $\tau$ ). At the non-polarized state, GeTe is a metal, the resulting SHC at the Fermi level is about  $100 \hbar/e(\Omega\text{cm})^{-1}$ . The value is peaked amount to  $110 \hbar/e(\Omega\text{cm})^{-1}$  at 0.2 eV above the Fermi level. Even larger values can be obtained at the energy around -2.0 eV below the Fermi level. We owe the SHC to the spin Berry curvature of the SOC band due to the equivalent SOC field because there is no Rashba effect. When the polarization increases, the SHC around the CBM decreases, and even changes to the negative value. This is due to that the Rashba effect leads to a negative SHC around the CBM and this value increases with the increase of the polarization. The increase of the SHC can be understood from the fact the Rashba constant increases with the electric field as shown already in Fig. 4. As can be seen from Eq.(2) and (5),  $\sigma_{xy}^z$  is an odd function of  $z$  and antisymmetric with respect to interchange of  $x$  and  $y$ . In this case, although the reversal of the polarization leads to the reversal of the spin vector winding, it does not lead to sign reversal of the SHC tensor. We have numerically checked the SHC values when the polarization is reversed and find that it remains when the electric polarization is reversed.

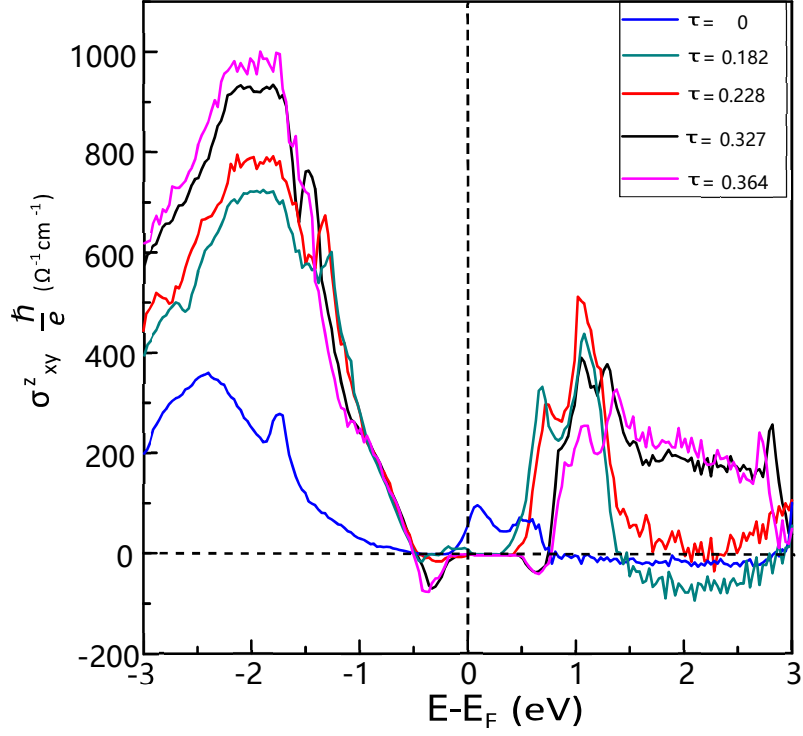


FIG. 6. The spin Hall conductivity  $\sigma_{xy}^z$  as the function of Te displacement ( $\tau$ ).

#### IV. Conclusions

To summarize, our theoretical calculations show that the spin texture is closely related to the ferroelectric polarization. When the ferroelectric polarization is reversed, the spin winding direction is reversed accordingly. This is due to the change of the equivalent coordinate system upon polarization reversal. It should be quite general in FERSC as shown in several compounds. The electric fields can be applied to tune the Rashba parameters. The SHCs have contributions from both the intrinsic SOC and Rashba effects while the latter can be easily tuned by the external electric fields. From the results we propose that the electric field is can be utilized to moderate the spin and electron transportation properties of FERSC materials. It provides a new dimension to design spintronic devices.

---

## Acknowledgments

W.X.Z. was supported from National Key R&D Program of China (No.2017YFB0406403).

---

\*Corresponding author.

xwzhang@uestc.edu.cn

- [1] T. Tanaka, H. Kontani, M. Naito, T. Naito, D. S. Hirashima, K. Yamada, J. Inoue, *Phys. Rev. B*, **2008** 77, 165117.
- [2] Y.K. Kato, R.C. Myers, A.C. Gossard, D.D. Awschalom, *Science*, **2004** 306, 1910.
- [3] Y.Y. Pai, A. Tylan-Tyler, P. Irvin, J. Levy, *Rep. Prog. Phys.*, **2018** 81,036503.
- [4] S. Datta, B. Das, *Appl. Phys. Lett.*, **1990** 56, 665.
- [5] W.Y. Choi, H. Kim, J. Chang, S.H. Han, A. Abbout, H.M. Saidaoui, A. Manchon, K.J. Lee, H.C. Koo, *Nano Letters*, **2018** 18, 7998.
- [6] W. Han, Y.C. Otani, S. Maekawa, *npj Quantum Mater.*, **2018** 3, 27.
- [7] E. Lesne, Y. Fu, S. Oyarzun, J. C. Rojas-Sánchez, D. C. Vaz, H. Naganuma, G. Sicoli, J.-P. Attané, M. Jamet, E. Jacquet, J.-M. George, A. Barthélémy, H. Jaffrès, A. Fert, M. Bibes, L. Vila, *Nat. Mater.*, **2016** 15, 1261.
- [8] V. L. Deringer, M. Lumeij, R. Dronskowski, *J. Phys. Chem. C*, **2012** 116,15801.
- [9] D.D. Sante, P. Barone, R. Bertacco, S. Picozzi, *Adv. Mater.*, **2012** 25, 509.
- [10] E. Plekhanov, P. Barone, D. Di Sante, S. Picozzi, *Phys. Rev. B*, **2014** 90, 161108.
- [11] E. Bruyer, D.D. Sante, P. Barone, A. Stroppa, M. Whangbo, S. Picozzi, *Phys. Rev. B*, **2016** 94, 195402.
- [12] D. Wu, L.D. Zhao, S. Hao, Q. Jiang, F. Zheng, J. W. Doak, H. Wu, H. Chi, Y. Gelbstein, C. Uher, C. Wolverton, M. Kanatzidis, J. He, *J. Am. Chem. Soc.*, **2014** 136, 11412.
- [13] M.J. Polking, M.G. Han, A. Yourdkhani, V. Petkov, Ch.F. Kisielowski, V. V. Volkov, Y. Zhu, G. Caruntu, A. P. Alivisatos, R. Ramesh, *Nat. Mater.*, **2012** 11, 700.
- [14] A. V. Kolobov, D. J. Kim, A. Giussani, P. Fons, J. Tominaga, R. Calarco, A. Gruverman, *APL Materials*, **2014** 2, 066101.
- [15] B.J. Kooi, B. Noheda, *Science*, **2016** 353, 221.
- [16] G. Bruns, P. Merkelbach, C. Schlockermann, M. Salanga, M. Wuttig, T. D. Happ, J. B. Philipp, M. Kund, *Appl. Phys. Lett.*, **2009** 95, 043108.

- 
- [17] J.E. Boschker, R. Wang, R. Calarco, *Cryst. Eng. Comm*, **2017** 19, 5324.
  - [18] C. Rinaldi, S. Varotto, M. Asa, J. Slawińska, J. Fujii, G. Vinai, S. Cecchi, D. D. Sante, R. Calarco, I. Vobornik, G. Panaccione, S. Picozzi, R. Bertacco, *Nano Lett.*, **2018** 18, 2751.
  - [19] L. L. Tao, T.R. Paudel, A.A. Kovalev, E.Y. Tsybal, *Phys. Rev. B*, **2017** 95, 245141.
  - [20] H. Maaß, H. Bentmann, C. Seibel, C. Tusche, S.V. Eremeev, T.R. F. Peixoto, *Nat. Comm.*, **2016** 7, 11621.
  - [21] Y.H. Meng, W. Bai, H. Gao, S. Gong, J. Wang, C. Duan, J. Chu *Nanoscale*, **2017** 9, 17957.
  - [22] C. Rinaldi, J. C. Rojas-Sánchez, R. N. Wang, Y. Fu, S. Oyarzun, L. Vila, S. Bertoli, M. Asa, L. Baldrati, M. Cantoni, J.-M. George, R. Calarco, A. Fert, R. Bertacco, *APL Materials*, **2016** 4, 032501.
  - [23] J.W. Park, S.H. Eom, H. Lee, J.L.F. Da Silva, Y.S. Kang, T.Y. Lee, Y.H. Khang, *Phys. Rev. B*, **2009** 80, 115209.
  - [24] U. V. Waghmare, N. A. Spaldin, H. C. Kpal, R. Seshadri, *Phys. Rev. B*, **2003** 67, 125111.
  - [25] D.J. Singh, *J. Appl. Phys.*, **2013** 113, 203101.
  - [26] G. S. Pawley, W. Cochran, R. A. Cowley, G. Dolling, *Phys. Rev. Lett.*, **1966** 17, 753.
  - [27] E.F Steigmeier, G Harbeke, *Solid State Comm.*, **1970** 8, 1275.
  - [28] R.E. Cohen, *Nature*, **1992** 358, 136.
  - [29] R. Resta, D. Vanderbilt, *Theory of Polarization: A Modern Approach*, in *Physics of Ferroelectrics: a Modern Perspective*, ed. by K.M. Rabe, C.H. Ahn, J.-M. Triscone (Springer-Verlag, **2007**, Berlin), 31-68.
  - [30] J. Krempaský, H. Volfová, S. Muff, N. Pilet, G. Landolt, M. Radović, M. Shi, D. Kriegner, V. Holý, J. Braun, H. Ebert, F. Bisti, V. A. Rogalev, V. N. Strocov, G. Springholz, J. Minár, J. H. Dil, *Phys. Rev. B*, 2016 94, 205111.
  - [31] J. Železný, H. Gao, Aurélien Manchon, Frank Freimuth, Yuriy Mokrousov, J. Zemen, J. Mašek, Jairo Sinova, T. Jungwirth, *Phys. Rev. B*, **2017** 95, 014403.
  - [32] G. Y. Guo, S. Murakami, T.-W. Chen, N. Nagaosa, *Phys. Rev. Lett.*, **2008** 100, 096401.
  - [33] J. Sinova, S. O. Valenzuela, J. Wunderlich, C.H. Back, T. Jungwirth, *Rev. Mod. Phys.*, **2015** 87, 1213.
  - [34] P. Giannozzi, Stefano Baroni, N. Bonini, M. Calandra, R. Car, C. Cavazzoni, D. Ceresoli, G.L. Chiarotti, M. Cococcioni, I. Dabo, A. D. Corso, S. Gironcoli, S. Fabris, G. Fratesi, R. Gebauer, U. Gerstmann, C. Gougoussis, A. Kokalj, M. Lazzeri, L. Martin-Samos, N. Marzari, F. Mauri, R. Mazzarello, S. Paolini, A. Pasquarello, L. Paulatto, C. Sbraccia, S. Scandolo, G. Sclauzero, A.P Seitsonen, A. Smogunov, P. Umari, R. M. Wentzcovitch, *J. Phys.: Cond. Matt.*, **2009** 21, 395502.

- 
- [35] J. P. Perdew, K. Burke, M. Ernzerhof, *Phys. Rev. Lett.*, **1996** 77, 3865.
- [36] *Atomistix ToolKit Version 4.0*, 2017, [online] Available: <http://www.quantumwise.com>.
- [37] <https://bitbucket.org/zeleznyj/wannier-linear-response/wiki/home>.